




# All normal dispersion nonlinear fibre supercontinuum source characterization and application in hyperspectral stimulated Raman scattering microscopy

PEDRAM ABDOLGHADER,<sup>1,2</sup> ADRIAN F. PEGORARO,<sup>1,2</sup> NICOLAS Y. JOLY,<sup>3,4</sup>  ANDREW RIDSDALE,<sup>2</sup>  RUNE LAUSTEN,<sup>2</sup> FRANÇOIS LÉGARÉ,<sup>5</sup> AND ALBERT STOLOW<sup>1,2,6,7,\*</sup>

<sup>1</sup>*Department of Physics, University of Ottawa, Ottawa, ON K1N 6N5, Canada*

<sup>2</sup>*Security and Disruptive Technologies, National Research Council Canada, Ottawa, ON K1A 0R6, Canada*

<sup>3</sup>*Max-Planck Institute for the Science of Light, Staudtstraße 2, 91058 Erlangen, Germany*

<sup>4</sup>*Department of Physics, IZNF, University of Erlangen-Nuremberg, Cauerstraße 3, 91058 Erlangen, Germany*

<sup>5</sup>*Institut National de la Recherche Scientifique, Centre EMT, ALLS Laboratory, Varennes, QC J3X1S2, Canada*

<sup>6</sup>*NRC-uOttawa Joint Centre for Extreme Photonics, Ottawa, ON K1N 6N5, Canada*

<sup>7</sup>*Max-Planck-uOttawa Centre for Extreme and Quantum Photonics, Ottawa, ON K1N 6N5, Canada*

\* [astolow@uottawa.ca](mailto:astolow@uottawa.ca)

**Abstract:** Hyperspectral stimulated Raman scattering (SRS) microscopy is a powerful label-free, chemical-specific technique for biomedical and mineralogical imaging. Usually, broad and rapid spectral scanning across Raman bands is required for species identification. In many implementations, however, the Raman spectral scan speed is limited by the need to tune source laser wavelengths. Alternatively, a broadband supercontinuum source can be considered. In SRS microscopy, however, source noise is critically important, precluding many spectral broadening schemes. Here we show that a supercontinuum light source based on all normal dispersion (ANDi) fibres provides a stable broadband output with very low incremental source noise. We characterized the noise power spectral density of the ANDi fibre output and demonstrated its use in hyperspectral SRS microscopy applications. This confirms the viability and ease of implementation of ANDi fibre sources for broadband SRS imaging.

© 2020 Optical Society of America under the terms of the [OSA Open Access Publishing Agreement](#)

## 1. Introduction

Coherent Raman microscopy (CRM) encompasses a family of nonlinear optical imaging techniques which provide label-free, chemical-selective, 3D sectioning of samples and has found use in fields ranging from biology, to medicine, to mineralogy [1–6]. Typically, Raman contrast is achieved with two ultrashort pulse input beams, designated Pump and Stokes, whose frequency difference is tuned to the Raman vibrational frequency of interest. Although Raman imaging based on a single vibrational resonance can be effective, non-resonant background signals and overlapping bands can reduce both contrast and chemical specificity in CRM. For target identification, tuning across the Raman spectrum is critical. For the case of modulation transfer schemes, other nonlinear optical processes, including two-photon absorption (TPA), excited-state absorption (ESA), cross phase modulation (XPM) and thermal lensing (TL), can couple the propagation of the Pump and Stokes beams and therefore appear as a modulated signal [7]. These background signals may even appear bright in an image but do not correspond Raman resonant signals and therefore reduce chemical-specific contrast. Single Raman shift imaging can be misleading: only by tuning across the Raman spectrum and identifying the

peaks can the optical response be confirmed as being Raman resonant [8]. For this reason, in many applications multiple Raman bands are scanned using either multiplex or hyperspectral Raman imaging [4,9–11]. In hyperspectral imaging, the instantaneous Pump-Stokes frequency difference must be tuned over the Raman spectral region of interest. For narrow band (picosecond) pulses, this can be achieved by tuning the center frequency of either the Pump or Stokes input lasers. Alternatively, spectral focussing of linearly chirped femtosecond (fs) pulses [12–17] can be applied, leading to rapid tuneability over the femtosecond laser bandwidth by scanning the time delay between the chirped pulses. In spectral focussing CRM, however, the Raman tuning range is limited by the bandwidths of the input fs sources. For example, synchronized fs oscillators or an fs oscillator/optical parametric oscillator (OPO) combination will typically have a rapid Raman tuning range of  $<300\text{ cm}^{-1}$ . To achieve broader Raman tuning ranges, the central frequency of one of the input fs lasers must be tuned, significantly reducing hyperspectral scan speeds. One approach to overcoming the bandwidth limitations of typical fs laser sources is to use supercontinuum generation in photonic crystal fibres (PCFs) in the anomalous dispersion regime, providing extremely broadband, temporally-synchronized outputs [14–16,18]. Two serious drawbacks of PCF-based sources for CRM are that (i) they offer relatively low output power and (ii) they typically have significant source noise (i.e. modulation instabilities) in RF spectral regions relevant to imaging [19,20]. For coherent anti-Stokes Raman scattering (CARS) microscopy applications, this added source noise is inconvenient but not limiting [18]. For stimulated Raman scattering (SRS) microscopy [1,2,21], however, source noise can be a serious limitation. Despite the drawbacks of low power and (potentially) high source noise, PCFs have found some application in SRS microscopy [15,16,22]. Further enhancements using balanced detection to reduce source noise [23–25] or active gain to increase power [26] offer possible routes to making the PCF sources more widely available, although at the cost of increased system complexity.

Here we show that all normal dispersion (ANDi) PCFs can generate a broad supercontinuum with minimal added noise while increasing the scan range to  $1000\text{ cm}^{-1}$  without having to tune any lasers and avoiding the need for balanced detection schemes. We also demonstrate their use as a simple source for hyperspectral SRS microscopy. As a short pulse propagates in an ANDi fibre, the spectral broadening it experiences is uniquely due to self-phase modulation [27,28], yielding a broad linearly chirped output spectrum with very small intensity fluctuations [29]. This process is highly efficient, providing high power throughput for imaging applications. Furthermore, it is a completely passive system which can be added to any standard spectral focussing SRS microscopy setup without the need of additional detectors or active optical components.

It is important to consider the various roles that the source noise spectrum can play in modulation transfer CRM [30]. There are typically two RF spectral regions of interest in laser scanning CRM. One is in a band around the modulation frequency, typically in the 1–10 MHz range. In this range, source noise in the modulated (non-detected) beam is unimportant: it becomes important, however, for the detected beam (vide infra). There is a second frequency range which is important for image formation in raster scanning laser microscopy. This is the noise spectral power in the range of the inverse pixel dwell time, typically in the 10–50 kHz range. The pixel dwell time acts like a low pass filter: it averages over all higher frequency noise but still remains affected by lower frequency (pixel-to-pixel) noise. In modulation transfer CRM, the signal power in the detected beam depends linearly on the input power of each of the Pump and Stokes beams. This means that, although the noise in the non-detected (modulated) beam around the (MHz) modulation frequency is unimportant, pixel-to-pixel variations in the average power of the non-detected beam will lead to level variations in the detected signal averaged over the pixel dwell time. These changes in the ‘quasi-DC’ signal level from pixel-to-pixel lead to a noisy ‘speckle-like’ image, despite a high signal-to-noise ratio (at the modulation frequency)

within a given pixel. As an illustration of this point, we previously demonstrated that kHz source noise can lead to detrimental ‘image speckle’ in an all-fibre CRM scheme [31].

In this paper, we present a standard stimulated Raman loss (SRL) scheme wherein the Stokes (here, ANDi-based) beam is modulated and the Pump loss signal is detected by a lock-in amplifier. In this case, the noise spectrum of the modulated Stokes is unimportant in the (MHz) modulation band. However, it can be advantageous (i.e. removes nonlinear absorption background) to use a simulated Raman gain (SRG) scheme [7], wherein the Pump is modulated and the gain in the Stokes is detected by a lock-in amplifier. In this implementation, the noise spectrum of the Stokes (here, ANDi-based) in the MHz range will matter greatly. Therefore, our demonstration of the low noise of the ANDi source in both the kHz (image formation) and MHz (modulation frequency) ranges will encourage its use in both SRL and SRG schemes.

## 2. Methods

The ANDi fibre used in the present study was manufactured from pure silica tubes by the conventional stack-and-draw technique [32]. An electron micrograph (SEM) of the end face of the ANDi fibre used here is shown in Fig. 1(a). The distance between the holes in the cladding is  $\Lambda = 1.42 \mu\text{m}$  and the hole diameter  $d$  is chosen so that  $d/\Lambda = 0.39$ . With these geometrical parameters, this fibre exhibits weak normal dispersion around the pump wavelength, as shown below in Fig. 1(b). The dispersion is evaluated using a semi-analytical approach [33]. A typical power-dependent spectrum for this ANDi fibre is shown in Fig. 1(c). In this demonstration, we launched a  $\sim 140$  fs duration pulse centred at 1042 nm wavelength at a 75.6 MHz repetition rate. The optimized input coupling efficiency was 65% and the maximum input pulse energy applied was 13.2 nJ, corresponding to 1 W input power. An example output spectrum generated using 254 mW input pump power is shown in Fig. 1(d). At this power, the 6 dB bandwidth is about 300 nm.

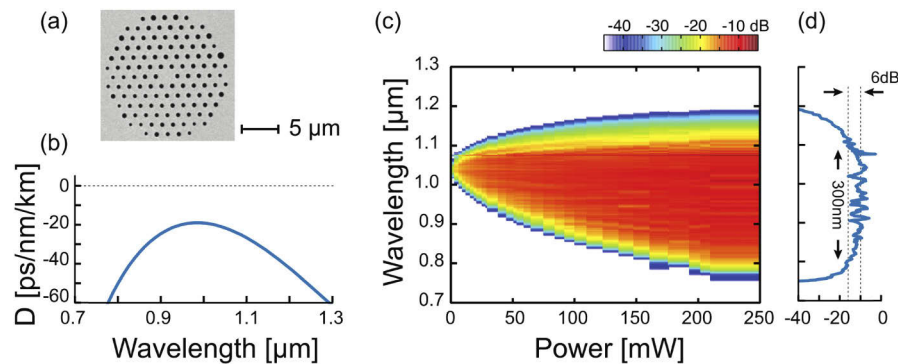


**Fig. 1.** (a) SEM of the end face of the ANDi fibre used here, (b) the calculated dispersion for this fibre, and (c) the experimental power-dependent output spectrum using a  $\sim 140$  fs pulse from an Yb-doped solid-state laser operating at 1042 nm, with pulse energies up to 13.2 nJ. (d) A typical output spectrum generated using 254 mW input pump power.

## 3. Experimental setup for RF spectral noise characterization

A schematic of the spectrally resolved noise measurement setup is shown in Fig. 2. All measurements were performed with a femtosecond dual output laser system (InSight DS+, Spectra-Physics, USA) that produced two synchronized pulse trains at 80 MHz. The fixed wavelength output centered at 1040 nm has a transform-limited pulse duration of 220 fs with an average power of 1 W, whereas the second output was tunable over the 680–1300 nm range

with a transform-limited pulse duration of approximately 180 fs and 1.5 W of average power. The 1040 nm output was sent through a variable beam splitter constructed from a half wave plate (HWP), (AHWP05M-980, Thorlabs, USA) and a polarizing beam splitter (PBS), (PBS102, Thorlabs, USA) before being passed through a Pockels cell (350-160, Conoptics, USA) used to impart a 1 MHz amplitude modulation. Another HWP was used to match the pump laser polarization to that of the fibre axis before it was focussed by an aspheric lens (C230TMD-B, Thorlabs) into the 10 cm long ANDi fibre (core diameter of 2.2  $\mu\text{m}$ ) shown in Fig. 1(a). The ANDi fibre alignment, in terms of spatial overlap and polarization axis, was optimized for maximum spectral broadening, (56–59% coupling efficiency). The ANDi fibre output was collimated by another aspheric lens (C340TMD-B, Thorlabs) and spectrally dispersed by a prism followed by an adjustable slit to select a narrow spectral band from the ANDi supercontinuum output. To allow for comparative noise measurements, the average power within each spectral band was kept constant using a variable neutral density (ND) filter (NDC-50C-2-B, Thorlabs). The central wavelength and bandwidth of each spectral band was determined using an optical spectrum analyzer (Ando AQ6315E). The pulse train of the selected band was measured by a Si photodiode (DET10A Thorlabs), the output of which was sent to a Zurich Instruments ultra-high-frequency lock-in (UHFLI) amplifier. The sweeper function (Amplitude Noise) of the UHFLI was used for all RF spectral noise measurements reported here.

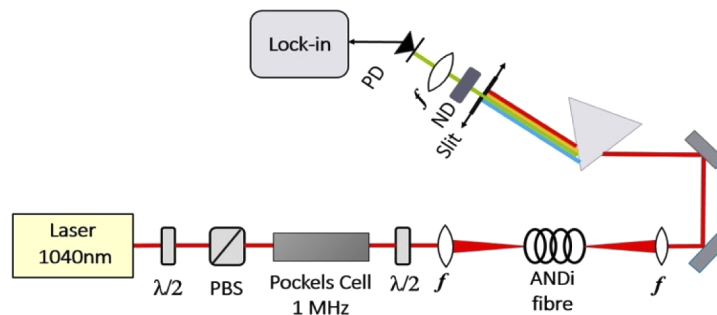


**Fig. 2.** A depiction of the spectrally resolved noise power spectral density (NPSD) measurement setup. This arrangement permits direct measurement of the NPSD in the RF (kHz-MHz) spectral domain within a selected optical bandpass (10 nm) of the ANDi fibre supercontinuum output. A neutral density filter (ND) ensured that the NPSD measurements were done at constant input optical power. Illustrated are the pump laser at 1040 nm, half wave plate ( $\lambda/2$ ), polarizing beam splitter (PBS), Pockels Cell (1 MHz), coupling/collimating lens ( $f$ ), ANDi fibre, adjustable optical bandpass slit, neutral density filter (ND), Si photodiode (PD), and lock in amplifier.

### 3.1. RF noise power spectral density

In SRS microscopy, which is typically based upon modulation transfer detection combined with a raster scanning technique for image generation, source noise can limit both (i) the signal-to-noise ratio (SNR) at the modulation frequency, and (ii) the pixel-to-pixel noise in the image. As discussed in the Introduction, the Stokes (here ANDi-based) source noise at the MHz modulation frequency is critical only when the stimulated Raman gain scheme is implemented. In contrast, the source noise at the inverse pixel dwell time (kHz) is always important in the image formation process. Here we implemented a stimulated Raman loss (SRL) scheme wherein the ANDi-based Stokes is modulated, and the loss of tunable Pump is detected by the lock-in amplifier. In this case, the noise spectrum of the modulated (ANDi) Stokes is unimportant in the (MHz) modulation band. However, for simulated Raman gain (SRG), the noise spectrum of the ANDi-based Stokes will matter greatly. Therefore, to quantitatively determine the suitability of an ANDi fibre source for

SRS microscopy, we characterized the noise of both the input laser and the ANDi supercontinuum output in RF regions around 1 MHz (a typical modulation frequency) and around 40 kHz (a typical inverse pixel dwell time) by measuring the RF noise power spectral density (NPSD in  $dBV/\sqrt{Hz}$ ). To ensure that the noise characteristics were relevant for SRS microscopy, the input laser was amplitude modulated with a 50% duty cycle at 1 MHz using a Pockels cell. For all noise measurements reported here, we used (following the Pockels cell modulator) 500 mW average power (12.5 nJ/pulse) in the 1040 nm pump beam. The measured NPSD in the 1 MHz range are shown in Fig. 3 for: the electronic noise floor; the input laser; and several different 10 nm spectral bands from the ANDi supercontinuum output. The electronic noise floor was measured with all input optical signals blocked. The average optical power at the Si photodiode within each 10 nm spectral band, and for the input pump laser, were set equal by adjusting the variable ND filter. To characterize the increase in noise due to supercontinuum generation, we report the “excess NPSD” which we define to be the average increase in NPSD compared to the electronic noise floor. In the 1 MHz range (0.9–1.1 MHz), we report the average NPSD by excluding the large Pockels Cell modulation peak at 1 MHz. Around 40 kHz (20–60 kHz), we report the average NPSD over the entire range. In Fig. 4, we show the excess NPSD for the different supercontinuum 10 nm-wide spectral bands (centered at 940, 962, 973, 1003, and 1020 nm) as well as that of the input laser (1040 nm) before transmission through the fibre. As expected, the input laser shows little excess NPSD at 1 MHz: 0.9  $dBV/\sqrt{Hz}$  above background. However, at 40 kHz the pump laser does show a measurable 1.7  $dBV/\sqrt{Hz}$  increase in NPSD. As seen in Fig. 4, all supercontinuum 10 nm spectral bands show increased excess NPSD relative to the input laser: these appear similar in both RF frequency ranges, varying from 3.7–14.2  $dBV/\sqrt{Hz}$ . However, the observed increases in excess NPSD are relatively low, suggesting that an ANDi source may be suitable for broadband SRS microscopy.

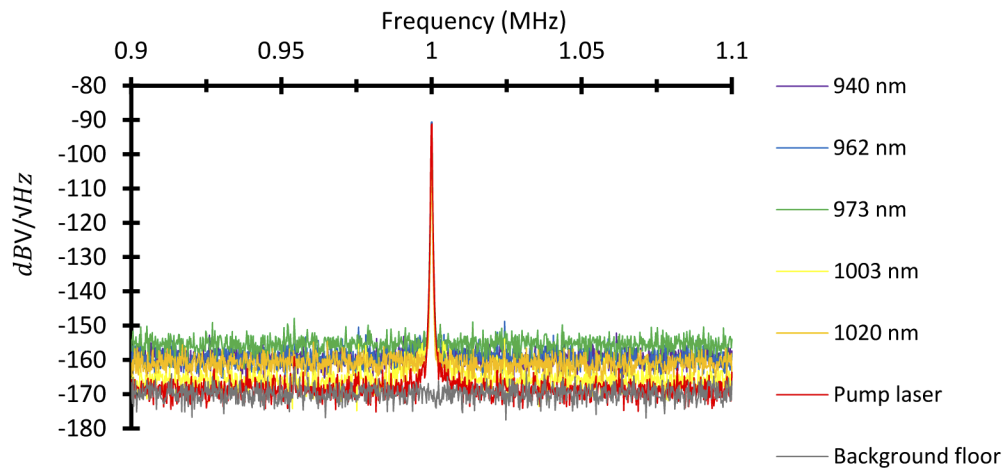


**Fig. 3.** RF noise power spectral density over [0.9–1.1] MHz at constant input optical power, shown for the electronic noise floor (gray, zero input), the 1040 nm laser (red), and as a function of 10 nm spectral band central wavelength.



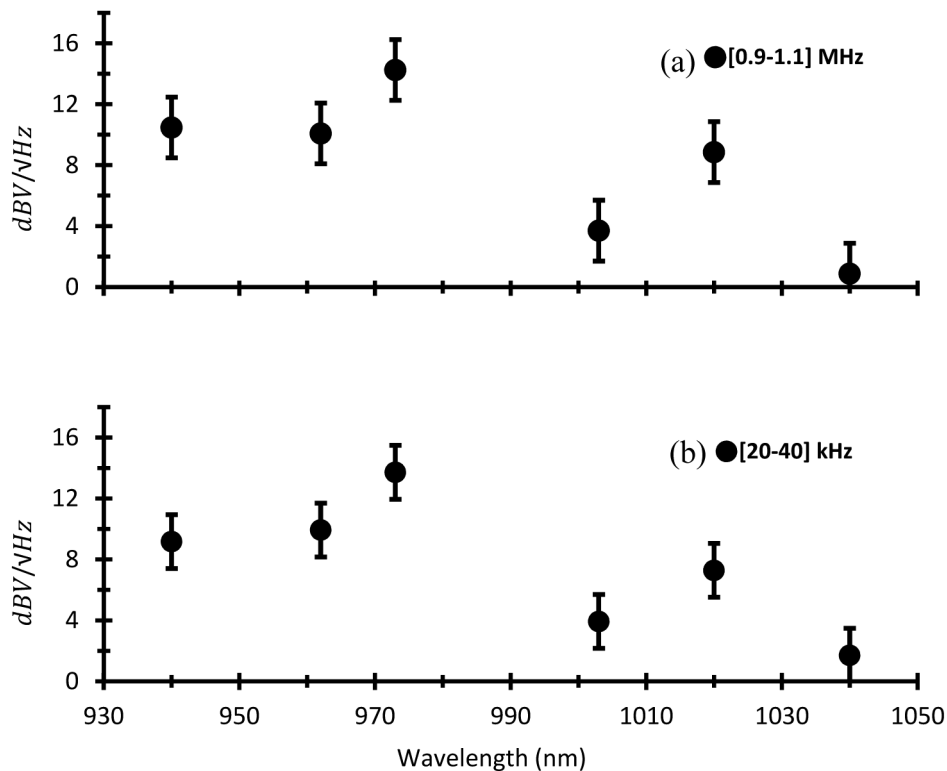


**Fig. 4.** Excess noise power spectral density relative to the electronic noise floor. Shown are the excess NPSD as a function of 10 nm spectral band central wavelength over (a) the 0.9–1.1 MHz range, (b) 20–40 kHz range.

#### 4. Hyperspectral stimulated Raman microscopy

In order to demonstrate the use of ANDi fibres for hyperspectral SRS microscopy, we used a modified broadband SRS spectral focusing arrangement, illustrated in Fig. 5. The InSight DS+ laser system provided a tunable output beam and a fixed wavelength beam (1040 nm), the latter used for supercontinuum generation in the ANDi fibre. The average power of each output was adjusted using a half-wave plate, (AHWP05M-980, Thorlabs, USA) and a polarizing beam splitter (PBS102, Thorlabs, USA). The input to the ANDi fibre was identical to that used for the spectrally-resolved noise measurements. After collimation, the fibre output was spectrally filtered (980 nm RazorEdge LP, Semrock) so as to remove all supercontinuum wavelengths below 980 nm. The supercontinuum output (acting here as the SRS Stokes beam) and the tunable InSight output (acting here as the SRS pump beam) were recombined on a dichroic mirror (DM), (DMLP 950, Thorlabs, USA). Both beams were linearly chirped by 60 cm of SF11 glass. This chirped pulse arrangement permits rapid tuning of the Raman resonant frequency by time-scanned spectral focusing. The time delay (which tunes the instantaneous Raman frequency) between the tunable pump and the supercontinuum Stokes beam was controlled by a retro-reflector mounted on a translation stage in the pump beam path. The recombined beams were sent to an inverted microscope (IX-71, Olympus, Japan) and focused into the sample with a near IR microscope objective (UPlanSapo, 20x, NA 0.75, Olympus, Japan). Galvanometer mirrors permitted raster scanning across the sample, thus providing an image. After the sample, the forward propagating beams were collected by a second objective acting as the condenser (LUMPlanFI/IR, 40x, NA 0.8 water immersion, Olympus, Japan). A function generator (DS345,

Stanford Research Systems, USA) provided the 1 MHz modulation signal for the Pockels cell. The modulation reference signal was sent to a lock-in amplifier (UHFLI, Zurich Instruments). The amplitude modulated supercontinuum beam was blocked by optical filters (FES0950 SP Thorlabs, FF01-940/SP-25 Semrock), and the transmitted pump beam was recorded using a large-area photodiode (FDS10X10, Thorlabs, USA). Typically, a few mW of optical power impinged onto the photodiode which was reverse biased at 50 V. The photodiode output electrical signal was filtered by an RF bandpass filter (#3128, KR Electronics) centred at 1 MHz frequency. The filtered signal was amplified by a transimpedance amplifier (DHPCA-100, Femto Messtechnik GmbH, Germany), providing the signal input to the lock-in amplifier. A lock-in time constant of 20  $\mu$ s was used, and the relative phase of the lock-in amplifier was adjusted for maximum SRS signal. Data collection and galvanometer synchronization was performed using ScanImage [34].

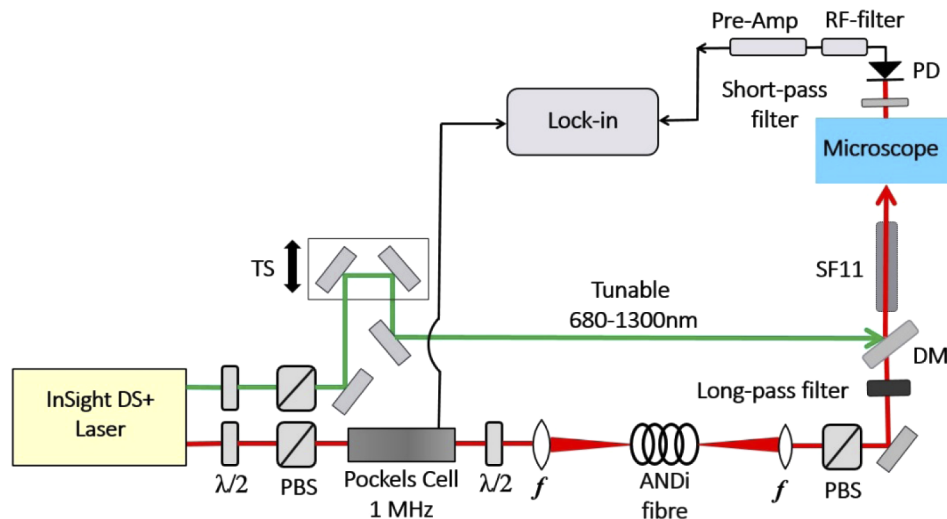


**Fig. 5.** The broadband hyperspectral stimulated Raman scattering (SRS) microscopy optical arrangement using the ANDi fibre source. In this experiment, the tunable output acted as the SRS pump, whereas the ANDi fibre output acted as the broadband SRS Stokes. Depicted are the: dual output laser system, half wave plate ( $\lambda/2$ ), polarizing beam splitter (PBS), Pockels cell (1 MHz), translation stage (TS), focussing/collimating aspheric lens ( $f$ ), All normal dispersion fibre as supercontinuum source (ANDi), dichroic mirror (DM), highly dispersive piece of glass (SF-11), RF-filter: electronic bandpass filter at 1 MHz central frequency, and photodiode (PD).

In order to normalize the recorded SRS spectra, we needed to determine the wavelength variation of optical power within the ANDi supercontinuum output. This can be routinely achieved by recording the sum-frequency of the instantaneous pump and Stokes frequencies. In the epi-direction, a dichroic mirror (720DCXXR, Chroma, USA) directed back-reflected sum frequency generation (SFG) signals through a short pass filter (750SP, Chroma, USA) in front of a photomultiplier tube (Hamamatsu H10723-01). Samples of KDP powder (data not shown) were used to generate a broadband SFG signal. Since both SFG and SRS are linear in the pump and Stokes powers, SFG can be used to normalize (as a function of Raman shift) the spectrally resolved SRS signals from samples.

#### 4.1. Hyperspectral SRS microscopy using ANDi fibres

In order to demonstrate the use of ANDi fibres for broadband hyperspectral SRS microscopy, we chose two samples: neat dimethyl sulfoxide (DMSO) liquid and acetaminophen powder. DMSO

has two well-known Raman vibrational resonances at  $2997\text{ cm}^{-1}$  and  $2919\text{ cm}^{-1}$ . To obtain an SRS spectrum, the pump beam was tuned to  $817\text{ nm}$  and both the pump and supercontinuum were adjusted to  $50\text{ mW}$  average power at the microscope input. The lock-in time constant was set to  $20\text{ }\mu\text{s}$  and the pixel dwell time was  $32\text{ }\mu\text{s}$ . The SRS spectrum was recorded over 94 frames with a spectral scan speed of  $\sim 3\text{ cm}^{-1}/\text{s}$  and each image took  $\sim 2.13$  seconds. An SRS spectrum of DMSO thus obtained, along with the spontaneous Raman spectrum of DMSO, is shown in Fig. 6. The lower energy peak of DMSO ( $2997\text{ cm}^{-1}$ ) was used for normalization to facilitate comparisons; we estimate the spectral resolution to be  $\sim 37\text{ cm}^{-1}$ , limited here by poor chirp matching [14,35]. This can be significantly improved by carefully matching the linear and higher order chirp parameters of the pump and Stokes beams (vide infra). We note, however, the current resolution suffices for many applications.

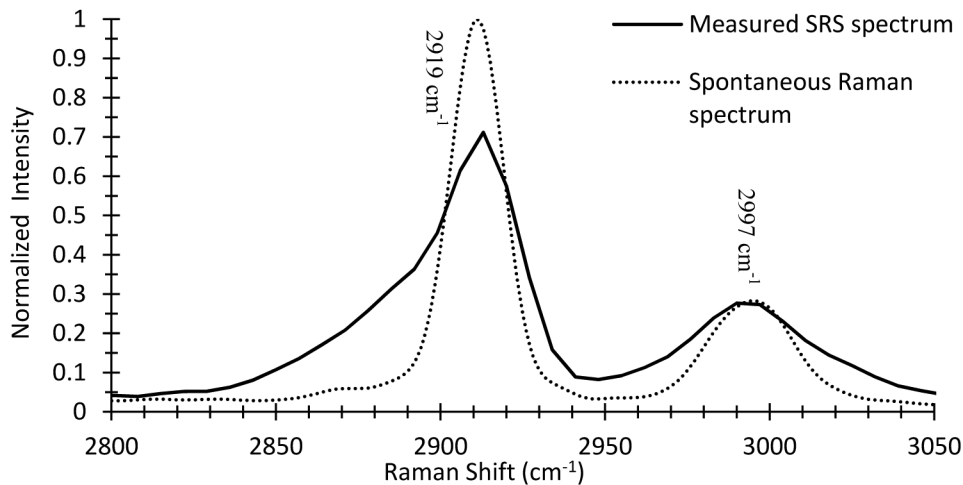


**Fig. 6.** Raman spectrum of DMSO recorded using SRS (solid line) and spontaneous Raman spectroscopy (dashed line) with the two main peaks in this region indicated. This demonstrates the utility of ANDi fibre sources for SRS spectroscopy. Normalization to peak height is based on the  $2997\text{ cm}^{-1}$  peak.

In order to demonstrate the broadband hyperspectral SRS microscopy imaging capability of this ANDi light source, we imaged acetaminophen powder which has many Raman resonances in the fingerprint region. In this case, the pump beam was tuned to  $910\text{ nm}$  ( $50\text{ mW}$  average power) whereas the broadband supercontinuum (Stokes beam) had  $60\text{ mW}$  of average power, measured at the microscope input. The data acquisition scheme was the same as was used for the DMSO experiment above. The SRS spectral scan was acquired over 259 frames with a spectral scan speed of  $6.85\text{ cm}^{-1}/\text{s}$  and each image took  $2.13\text{ s}$ . Hyperspectral SRS imaging of acetaminophen powder was recorded in the forward direction and normalized by an independently recorded SFG spectrum to correct for the spectral power dependence of the Stokes beam. At  $500\text{ mW}$  ANDi input power ( $12.5\text{ nJ/pulse}$ ,  $50\%$  duty cycle), the output Stokes bandwidth supported a continuous SRS tuning range of approximately  $860\text{--}1650\text{ cm}^{-1}$ . Importantly, this broad tuning range was achieved without tuning any input laser sources. A typical image is shown in Fig. 7(a). As discussed above, due to the limited applied chirp and the resulting mismatch of the pump and Stokes chirps, the Raman spectral resolution in this proof-of-concept demonstration is unoptimized. Corrections to the linear and the higher order chirp terms can lead to considerably improved Raman spectral resolution [35]. We emphasize, however, that this is not a limitation of the ANDi fibre source itself. The individual microcrystallites of acetaminophen were randomly



oriented within the sample and therefore the relative intensities of the Raman peaks, which are in general orientation-dependent, is not meaningful here.

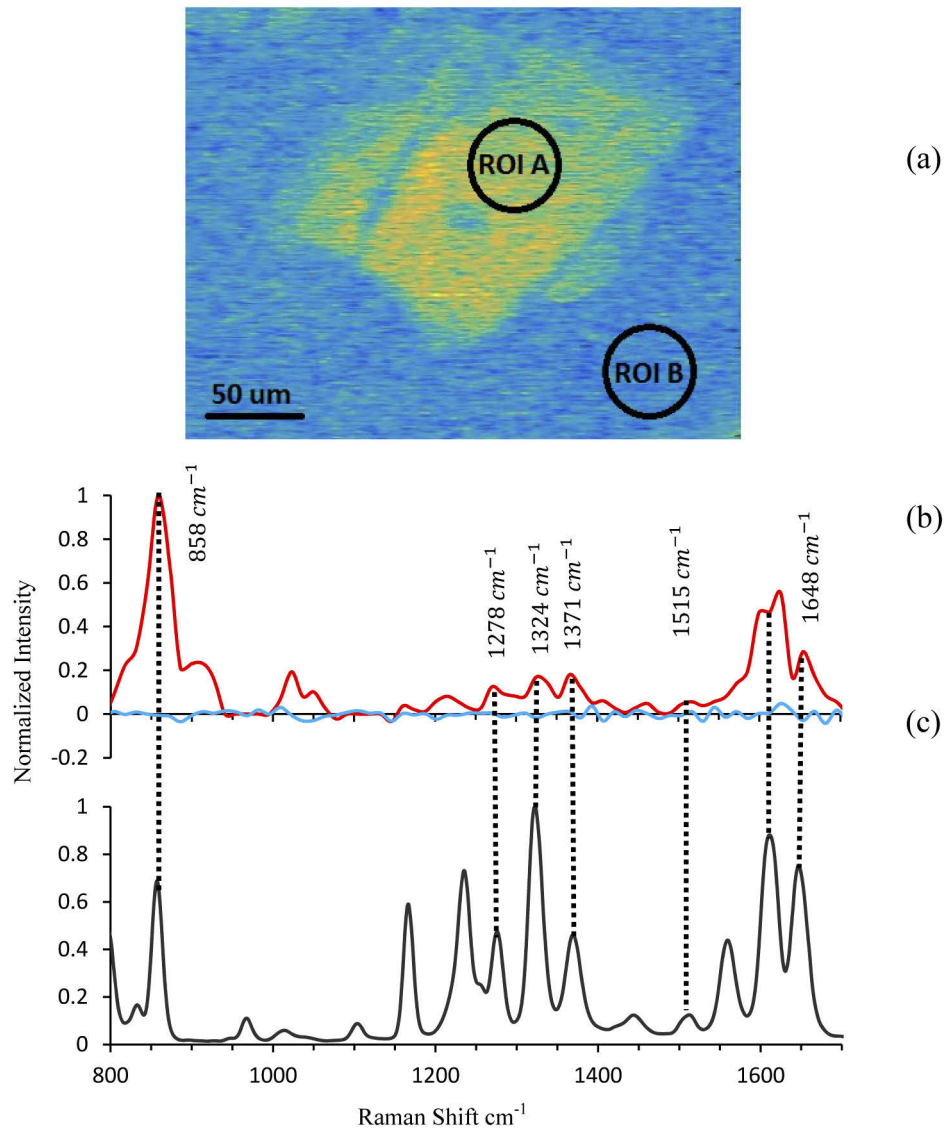


**Fig. 7.** (a) Normalized hyperspectral SRS microscopy image of a single acetaminophen micro-crystal. (b) The SRS Raman spectra of two Regions of Interest (ROI) are shown for the acetaminophen crystal (A, Red) and the background (B, Blue). (c) Spontaneous Raman spectrum of acetaminophen. A few of the peaks in the acetaminophen Raman spectrum are labelled in both (b) and (c), as indicated by the dashed lines.

Finally, in order to demonstrate the power of ANDi-based hyperspectral SRS Microscopy for label-free chemical-specific image contrast, we applied spectral cross correlation of the acetaminophen Raman spectrum to the whole image shown in Fig. 7(a): the spectral cross-correlation will maximize when a given pixel contains Raman peaks which match those of acetaminophen. Using spectral pattern recognition, we looked for pixels which contain the set of Raman peaks (not a single peak) assigned to the target species. This approach we

termed spectral cross-correlation and was used here to generate enhanced image contrast in a molecule-selective manner: it is based on the Raman spectrum of the target species in the spectral band of interest. The processed image is shown in Fig. 8. The contrast with respect to the background is much improved. We note that, in this case, the spectral cross correlation acts largely as a non-resonant background subtraction method. However, more generally, the power of the spectral cross-correlation approach is that it permits image contrast based on small changes in the Raman spectrum rather than in a single peak, such as those due to changes in the local chemical environment.

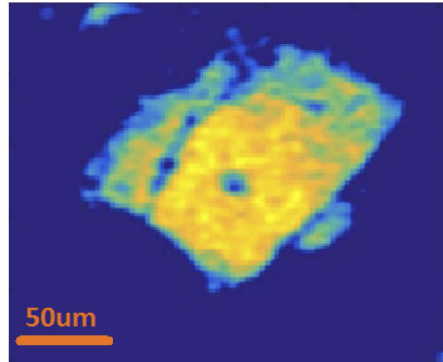


**Fig. 8.** Spectral cross-correlation of the image from Fig. 7(a) with the acetaminophen Raman spectrum shown in Fig. 7(b). The cross-correlation maximizes when a given pixel contains a Raman spectrum with sets of peaks matching those of Fig. 7(b). The image contrast with respect to background is greatly increased.

## 5. Conclusion

In hyperspectral SRS microscopy, the ability to rapidly scan over a wide range of Raman shifts is restricted because of the limited bandwidth of the laser sources available. We have shown that, using an ANDi fibre, it is possible to greatly increase the bandwidth of one of the laser sources without any significant increase in source noise that would otherwise have a deleterious effect on SRS performance. Using this setup, we were able to achieve hyperspectral Raman imaging over a  $800\text{ cm}^{-1}$  scan range without tuning either laser: in spectral focussing, the Raman spectrum is scanned simply by changing the time delay between pulses. Several improvements could be made to our current proof-of-concept setup in order to further enhance its utility. The Raman spectral resolution in spectral focussing SRS is determined by the degree of linear chirp and the matching of the Pump and Stokes chirp rates. We and others have previously demonstrated that spectral focussing SRS can have spectral resolution on the order of  $10\text{ cm}^{-1}$  via optimization of the chirp rate. The ability to optimize the chirp rate is sometimes limited by higher order dispersion; we find that the ANDi continuum output has minimal higher order dispersion based on our measurements of broad Raman spectra (i.e. the conversion of pulse time delay to wavenumber is linear). The current spectral scan range,  $>800\text{ cm}^{-1}$ , could also be increased. The output of the ANDi fibre on the blue side extends to  $<930\text{ nm}$  with reasonable output power and low noise but our current implementation truncates this spectrum due available optical filters. Extending the Stokes spectrum to below  $930\text{ nm}$ , would further extend the spectral scan range of the ANDi fibre source. Alternatively, rather than increasing the scan range, the spectral energy density of the continuum (i.e. the power per nm of bandwidth) can be increased at the expense of total bandwidth. For continuum generation in ANDi fibres, the total bandwidth depends on the peak power, not the input pulse duration [36]. In the proof-of-concept demonstration presented here,

we operated at maximum broadening which presents the challenge that the degree of noise often increases with nonlinearity. This demonstrated that hyperspectral SRS imaging is feasible even with the increased noise at maximal broadening. Alternatively, one could operate with less spectral broadening simply by applying a positive chirp to the ANDi fibre pump pulse. This will increase the power per unit bandwidth in the continuum and concomitantly decrease the NPSD, allowing for higher signal-to-noise ratio imaging across a narrower bandwidth of interest. The ANDi fibre operating conditions may be readily optimized for different applications without any change in hardware. In a future research direction, we plan to investigate a new type of polarization-maintaining ANDi fibre which we anticipate will have much improved power spectral density in its output. In conclusion, we have characterized the Noise Spectral Power Density of an ANDi fibre and demonstrated its utility as a simple, flexible and readily implemented source for broadband hyperspectral SRS microscopy.

## Funding

Natural Sciences and Engineering Research Council of Canada ; NRC-uO Joint Centre for Extreme Photonics; Max-Planck-uOttawa Centre for Extreme and Quantum Photonics.

## Acknowledgements

AS and NYJ thank the Max-Planck-uOttawa Centre for Extreme and Quantum Photonics for support and Prof. P. St.J. Russell and Dr. Francesco Tani for helpful discussions and Markus Lippl with providing data on the SC source.

## Disclosures

The authors declare that there are no conflicts of interest related to this article.

## References

1. J.-X. Cheng and X. S. Xie, *Coherent Raman Scattering Microscopy* (CRC Press, 2013).
2. J.-X. Cheng and X. S. Xie, "Vibrational spectroscopic imaging of living systems: An emerging platform for biology and medicine," *Science* **350**(6264), aaa8870 (2015).
3. C. Zhang, D. Zhang, and J.-X. Cheng, "Coherent Raman Scattering Microscopy in Biology and Medicine," *Annu. Rev. Biomed. Eng.* **17**(1), 415–445 (2015).
4. D. Polli, V. Kumar, C. M. Valensise, M. Marangoni, and G. Cerullo, "Broadband Coherent Raman Scattering Microscopy," *Laser Photonics Rev.* **12**(9), 1800020 (2018).
5. C. Zhang and J.-X. Cheng, "Perspective: Coherent Raman scattering microscopy, the future is bright," *APL Photonics* **3**(9), 090901 (2018).
6. M. C. Kao, A. F. Pegoraro, D. M. Kingston, A. Stolow, W. C. Kuo, P. H. J. Mercier, A. Gogoi, F. J. Kao, and A. Ridsdale, "Direct mineralogical imaging of economic ore and rock samples with multi-modal nonlinear optical microscopy," *Sci. Rep.* **8**(1), (2018).
7. P. Berto, E. R. Andresen, and H. Rigneault, "Background-free stimulated Raman spectroscopy and microscopy," *Phys. Rev. Lett.* **112**(5), 053905 (2014).
8. M. A. Houle, R. C. Burruss, A. Ridsdale, D. J. Moffatt, F. Légaré, and A. Stolow, "Rapid 3d chemical-specific imaging of minerals using stimulated raman scattering microscopy," *J. Raman Spectrosc.* **48**(5), 726–735 (2017).
9. C. H. Camp Jr and M. T. Cicerone, "Chemically sensitive bioimaging with coherent Raman scattering," *Nat. Photonics* **9**(5), 295–305 (2015).
10. T. W. Kee and M. T. Cicerone, "Simple approach to one-laser, broadband coherent anti-Stokes Raman scattering microscopy," *Opt. Lett.* **29**(23), 2701–2703 (2004).
11. H. Kano and H. -O. Hamaguchi, "Ultrabroadband (>2500cm<sup>-1</sup>) multiplex coherent anti-Stokes Raman scattering microspectroscopy using a supercontinuum generated from a photonic crystal fiber," *Appl. Phys. Lett.* **86**(12), 121113 (2005).
12. T. Hellerer, A. M. K. Enejder, and A. Zumbusch, "Spectral focusing: High spectral resolution spectroscopy with broad-bandwidth laser pulses," *Appl. Phys. Lett.* **85**(1), 25–27 (2004).
13. I. Rocha-Mendoza, W. Langbein, and P. Borri, "Coherent anti-Stokes Raman microspectroscopy using spectral focusing with glass dispersion," *Appl. Phys. Lett.* **93**(20), 201103 (2008).
14. A. F. Pegoraro, A. Ridsdale, D. J. Moffatt, Y. Jia, J. P. Pezacki, and A. Stolow, "Optimally chirped multimodal CARS microscopy based on a single Ti:sapphire oscillator," *Opt. Express* **17**(4), 2984–2996 (2009).

15. E. R. Andresen, P. Berto, and H. Rigneault, "Stimulated Raman scattering microscopy by spectral focusing and fiber-generated soliton as Stokes pulse," *Opt. Lett.* **36**(13), 2387–2389 (2011).
16. H. T. Beier, G. D. Noojin, and B. A. Rockwell, "Stimulated Raman scattering using a single femtosecond oscillator with flexibility for imaging and spectral applications," *Opt. Express* **19**(20), 18885–18892 (2011).
17. D. Fu, G. Holtom, C. Freudiger, X. Zhang, and X. S. Xie, "Hyperspectral Imaging with Stimulated Raman Scattering by Chirped Femtosecond Lasers," *J. Phys. Chem. B* **117**(16), 4634–4640 (2013).
18. J. G. Porquez, R. A. Cole, J. T. Tabarangao, and A. D. Slepков, "Brighter CARS hypermicroscopy via "spectral surfing" of a Stokes supercontinuum," *Opt. Lett.* **42**(12), 2255–2258 (2017).
19. F. Lu and W. H. Knox, "Generation of a broadband continuum with high spectral coherence in tapered single-mode optical fibers," *Opt. Express* **12**(2), 347–353 (2004).
20. A. M. Zheltikov, *Physics-Uspekhi* **49**, 605 (2006).
21. C. W. Freudiger, W. Min, B. G. Saar, S. Lu, G. R. Holtom, C. He, J. C. Tsai, J. X. Kang, and X. S. Xie, "Label-Free Biomedical Imaging with High Sensitivity by Stimulated Raman Scattering Microscopy," *Science* **322**(5909), 1857–1861 (2008).
22. K. Seto, Y. Okuda, E. Tokunaga, and T. Kobayashi, "Development of a multiplex stimulated Raman microscope for spectral imaging through multi-channel lock-in-detection," *Rev. Sci. Instrum.* **84**(8), 083705 (2013).
23. K. Nose, Y. Ozeki, T. Kishi, K. Sumimura, N. Nishizawa, K. Fukui, Y. Kanematsu, and K. Itoh, "Sensitivity enhancement of fiber-laser-based stimulated Raman scattering microscopy by collinear balanced detection technique," *Opt. Express* **20**(13), 13958–13965 (2012).
24. A. Gambetta, V. Kumar, G. Grancini, D. Polli, R. Ramponi, G. Cerullo, and M. Marangoni, "Fiber-format stimulated-Raman-scattering microscopy from a single laser oscillator," *Opt. Lett.* **35**(2), 226–228 (2010).
25. C. W. Freudiger, W. Yang, G. R. Holtom, N. Peyghambarian, X. S. Xie, and K. Q. Kieu, "Stimulated Raman scattering microscopy with a robust fibre laser source," *Nat. Photonics* **8**(2), 153–159 (2014).
26. B. Figueroa, W. Fu, T. Nguyen, K. Shin, B. Manifold, F. Wise, and D. Fu, "Broadband hyperspectral stimulated Raman scattering microscopy with a parabolic fiber amplifier source," *Biomed. Opt. Express* **9**(12), 6116–6131 (2018).
27. G. Agrawal, *Nonlinear Fiber Optics* (Academic Press, 2013).
28. A. M. Heidt, A. Hartung, G. W. Bosman, P. Krok, E. G. Rohwer, H. Schwoerer, and H. Bartelt, "Coherent octave spanning near-infrared and visible supercontinuum generation in all-normal dispersion photonic crystal fibers," *Opt. Express* **19**(4), 3775–3787 (2011).
29. A. M. Heidt, "Pulse preserving flat-top supercontinuum generation in all-normal dispersion photonic crystal fibers," *J. Opt. Soc. Am. B* **27**(3), 550–559 (2010).
30. X. Audier, S. Heuke, P. Volz, I. Rimke, and H. Rigneault, "Noise in stimulated Raman scattering measurement: From basics to practice," *APL Photonics* **5**(1), 011101 (2020).
31. A. F. Pegoraro, A. Ridsdale, D. J. Moffatt, J. P. Pezacki, B. K. Thomas, L. Fu, L. Dong, M. E. Fermann, and A. Stolow, "All-fiber CARS microscopy of live cells," *Opt. Express* **17**(23), 20700–20706 (2009).
32. P. S. J. Russell, "Photonic-Crystal Fibers," *J. Lightwave Technol.* **24**(12), 4729–4749 (2006).
33. K. Saitoh and M. Koshiba, "Empirical relations for simple design of photonic crystal fibers," *Opt. Lett.* **13**(1), 267–274 (2005).
34. T. A. Pologruito, B. L. Sabatini, and K. Svoboda, *Biomed. Eng. Online* **2**, 13 (2003).
35. M. Mohseni, C. Polzer, and T. Hellerer, "Resolution of spectral focusing in coherent Raman imaging," *Opt. Express* **26**(8), 10230–10241 (2018).
36. A.M. Heidt, A. Hartung, and H. Bartelt, *The Supercontinuum Laser Source*, (Springer, 2016).